Electronic Supplementary Materials:

For https://doi.org/10.1631/jzus.A2200203

FVM-based numerical simulation method for hydraulic fracture initiation in the rock around perforation

Yu ZHANG[1], Shaohao HOU[1], Songhua MEI[2], Yanan ZHAO[2], Dayong LI[1]

[1]*College of Pipeline and Civil Engineering, China University of Petroleum (East China), Qingdao 266580, China*

[2]*Hunan Provincial Key Laboratory of Key Technology on Hydropower Development, Zhongnan Engineering Corporation, Changsha 410014, China*

Section S1 Thermo-poro-elastic model and fracture initiation criteria

S1.1 Thermo-poro-elastic model

(1) The in-situ stress:

$$\sigma_{\text{in-situ}}=\begin{cases}\sigma_r=\dfrac{(\sigma_{\mathrm{H}}+\sigma_{\mathrm{h}})}{2}(1-\dfrac{r_{\mathrm{w}}{}^2}{r^2})+\dfrac{(\sigma_{\mathrm{H}}-\sigma_{\mathrm{h}})}{2}(1-\dfrac{4r_{\mathrm{w}}{}^2}{r^2}+\dfrac{3r_{\mathrm{w}}{}^4}{r^4})\cos 2\theta\\ \sigma_\theta=\dfrac{(\sigma_{\mathrm{H}}+\sigma_{\mathrm{h}})}{2}(1+\dfrac{r_{\mathrm{w}}{}^2}{r^2})-\dfrac{(\sigma_{\mathrm{H}}-\sigma_{\mathrm{h}})}{2}(1+\dfrac{3r_{\mathrm{w}}{}^4}{r^4})\cos 2\theta\\ \sigma_z=\sigma_{\mathrm{v}}-2\mu(\sigma_{\mathrm{H}}-\sigma_{\mathrm{h}})\cos 2\theta\\ \tau_{r\theta}=-\dfrac{(\sigma_H-\sigma_h)}{2}\left(1+\dfrac{2r_w^2}{r^2}-\dfrac{3r_w^4}{r^4}\right)\sin 2\theta\\ \tau_{rz}=\tau_{\theta z}=0\end{cases}, \tag{S1}$$

where $\sigma_r,\sigma_\theta,\sigma_z$ are the three–way positive stress, $\tau_{r\theta},\tau_{rz},\tau_{z\theta}$ are the shear stress, r_w is the radius of the wellbore, σ_H,σ_h are the horizontal maximum and minimum principal stress.

(2) Hydraulic induced stress:

$$\sigma_{\text{hydraulic}}=\begin{cases}\sigma_r=\dfrac{\alpha(1-2\mu)}{(1-\mu)}\dfrac{1}{r^2}\displaystyle\int_{r_{\mathrm{w}}}^{r}(P(r)-P_0)r\mathrm{d}r-\phi(P(r)-P_0)+P_{\mathrm{w}}\dfrac{r_{\mathrm{w}}^2}{r^2}\\ \sigma_\theta=-\dfrac{\alpha(1-2\mu)}{(1-\mu)}\dfrac{1}{r^2}\displaystyle\int_{r_{\mathrm{w}}}^{r}(P(r)-P_0)r\mathrm{d}r+(\alpha\dfrac{1-2\mu}{1-\mu}-\phi)(P(r)-P_0)-P_{\mathrm{w}}\dfrac{r_{\mathrm{w}}^2}{r^2},\\ \sigma_z=(\alpha\dfrac{1-2\mu}{1-\mu}-\phi)(P(r)-P_0)\end{cases} \tag{S2}$$

where θ is the polar angle in the direction of the maximum horizontal stress; ϕ is the effective porosity; α is the biot's coefficient, P_{w} is fluid pressure in the wellbore, P_0 is initiation pore pressure, μ is Poisson's ratio.

(3) Thermally induced stress:

$$\sigma_{\text{thermally}}=\begin{cases}\sigma_{\mathrm{r}}=-\dfrac{\alpha_m E}{3(1-2\mu)r^2}\displaystyle\int_{r_{\mathrm{w}}}^{r}T_H r\mathrm{d}r\\ \sigma_\theta=-\dfrac{\alpha_m E}{3(1-2\mu)}\left[\dfrac{1}{r^2}\displaystyle\int_{r_{\mathrm{w}}}^{r}T_H r\mathrm{d}r-T_H\right],\\ \sigma_{\mathrm{z}}=-\dfrac{\alpha_m E}{3(1-2\mu)}T_H\end{cases} \tag{S3}$$

where α_m is the coefficient of thermal expansion; T_H is the temperature function, $T_H=18+0.036H$, H is depth.

The temperature of the wellbore and perforation wall is assumed to be equal to the fluid injection temperature, then the stress components are expressed as follows considering the effect of porosity and initial pressure (Farahani et al., 2006):

$$\begin{aligned}\sigma_r &= P_{\mathrm{w}}\frac{r_{\mathrm{w}}^2}{r^2} + \delta\frac{\eta}{r^2}\int_{r_{\mathrm{w}}}^{r}(P(r)-P_0)r\mathrm{d}r - \phi(P(r)-P_0) - \frac{\eta_T}{r^2}\int_{r_{\mathrm{w}}}^{r}T_H r\mathrm{d}r \\ &+ \frac{(\sigma_{\mathrm{H}}-\sigma_{\mathrm{h}})}{2}(1-\frac{4r_{\mathrm{w}}^2}{r^2}+\frac{3r_{\mathrm{w}}^4}{r^4})\cos 2\theta + \frac{\sigma_{\mathrm{H}}+\sigma_{\mathrm{h}}}{2}(1-\frac{r_{\mathrm{w}}^2}{r^2}),\end{aligned} \tag{S4}$$

$$\begin{aligned}\sigma_\theta &= -P_w\frac{r_{\mathrm{w}}^2}{r^2} - \delta\left[(\eta-\phi)(P(r)-P_0) + \frac{\eta}{r^2}\int_{r_{\mathrm{w}}}^{r}(P(r)-P_0)r\mathrm{d}r\right] \\ &- \frac{\eta_T}{r^2}(\int_{r_{\mathrm{w}}}^{r}T_H r\mathrm{d}r - T_H) + \frac{\sigma_{\mathrm{H}}+\sigma_{\mathrm{h}}}{2}(1+\frac{r_{\mathrm{w}}^2}{r^2}) \\ &- \frac{(\sigma_H-\sigma_h)}{2}(1+\frac{3r_w^4}{r^4})\cos 2\theta,\end{aligned} \tag{S5}$$

$$\sigma_z = \sigma_v - 2\mu(\sigma_{\mathrm{H}}-\sigma_{\mathrm{h}})\frac{r_{\mathrm{w}}^2}{r^2}\cos 2\theta + (\eta-\phi)(P(r)-P_0) - \eta_{\mathrm{T}}T_H, \tag{S6}$$

$$\tau_{r\theta} = -\frac{(\sigma_{\mathrm{H}}-\sigma_{\mathrm{h}})}{2}\left(1+\frac{2r_{\mathrm{w}}^2}{r^2}-\frac{3r_{\mathrm{w}}^4}{r^4}\right)\sin 2\theta, \tag{S7}$$

$$\tau_{rz} = \tau_{r\theta} = 0, \tag{S8}$$

$$\eta = \alpha\frac{1-2\mu}{1-\mu}, \tag{S9}$$

$$\eta_{\mathrm{T}} = \frac{\alpha_{\mathrm{m}}E}{3(1-\mu)}, \tag{S10}$$

where $\delta = 1$ when the wellbore wall is permeable, $\delta = 0$ conversely;

Given that the perforation and the wellbore are orthogonal, the stress distribution around perforation is obtained from the stress distribution around wellbore by using coordinate transformation (Fig. S1):

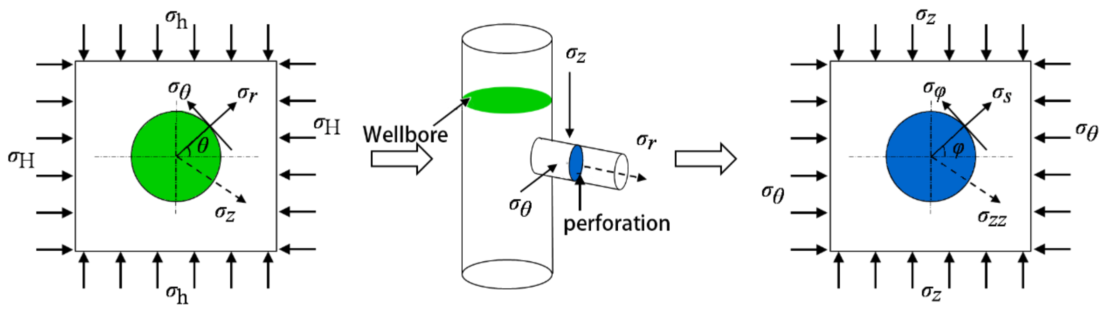

Fig. S1 Mechanical model and coordinate transformation

$$\begin{aligned}\sigma_s &= P_w\frac{s_{\mathrm{w}}^2}{s^2} + \frac{\eta}{r^2}\int_{r_{\mathrm{w}}}^{r}(P(r)-P_0)rdr - \phi(P(r)-P_0) + \\ &\frac{(\sigma_\theta-\sigma_z)}{2}(1-\frac{4s_{\mathrm{w}}^2}{s^2}+\frac{3s_{\mathrm{w}}^4}{s^4})\cos 2\varphi + \frac{\sigma_z+\sigma_\theta}{2}(1-\frac{s_{\mathrm{w}}^2}{s^2}),\end{aligned} \tag{S11}$$

$$\begin{aligned}\sigma_\varphi &= -P_w\frac{s_{\mathrm{w}}^2}{s^2} + (\eta-\phi)(P(r)-P_0) - \frac{\eta}{r^2}\int_{r_{\mathrm{w}}}^{r}(P(r)-P_0)rdr \\ &+ \frac{\sigma_z+\sigma_\theta}{2}(1+\frac{s_{\mathrm{w}}^2}{s^2}) - \frac{(\sigma_\theta-\sigma_z)}{2}(1+\frac{3s_{\mathrm{w}}^4}{s^4})\cos 2\varphi,\end{aligned} \tag{S12}$$

$$\sigma_{zz} = \sigma_r - 2\mu(\sigma_\theta - \sigma_z)\frac{s_w^2}{s^2}\cos 2\theta + (\eta - \phi)(P(r) - P_0), \tag{S13}$$

$$\tau_{zz\varphi} = 2\tau_{r\theta}\sin\varphi, \tag{S14}$$

$$\tau_{szz} = \tau_{s\varphi} = 0, \tag{S15}$$

where $\sigma_s, \sigma_\varphi, \sigma_{zz}$ are the radial, circumferential and axial stress of the perforation in the column coordinate system, respectively; s_w is the radius of the wellbore; φ is the angle between σ_s and σ_φ; $\tau_{zz\varphi}, \tau_{szz}, \tau_{s\varphi}$ are the shear stress.

S1.2 Fracture initiation criteria

The fracture initiates when a principal tensile stress exceeds the tensile strength of rock or the perforation wall in the maximal horizontal direction fractures first as the perforation azimuth rises. The maximum tensile stress is the extreme value of the third principal stress σ_3 for the perforation azimuth φ, Then Eq. (S16) is used to determine the fracture pressure and location.

$$\begin{cases} \sigma_{3,\min} - \alpha P = -\sigma_t \\ \sigma_\theta' = \sigma_\theta - \alpha P = -\sigma_t \end{cases}, \tag{S16}$$

Based on the thermo-poro-elastic model and fracture initial criterion, a hydraulic fracturing initiation model algorithm is proposed as Fig. S2.

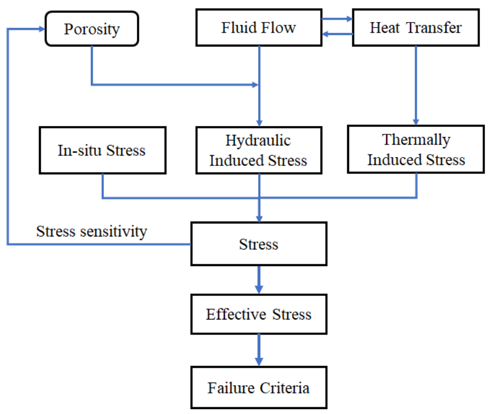

Fig. S2 Hydraulic fracturing initiation model algorithm

Section S2 Analysis of relevant parameters and stress sensitivity

Experimental studies have found that the flow velocity alone cannot determine the state of fluid flow. Therefore, Reynolds number (*Re*) is used to divide the flow state in reservoir into two regions: the linear laminar zone (*Re*<10) and the turbulent zone (*Re*>10). The dimensionless quantity *Re* is defined as:

$$Re = \frac{\rho_w d v}{\phi\mu}, \tag{S17}$$

where *v* is the fluid flow rate; ρ_w is the fluid density; *d* is a characteristic length, taking the equivalent diameter.

In the beginning of hydraulic fracturing, the fluid flow is regarded as laminar flow when *Re*<10, and the flow velocity is proportional to the pressure gradient:

$$-\frac{dP}{dX}=\frac{\mu}{K}v, \tag{S18}$$

where X is the direction of flow.

As the fluid pressure keeps increasing, the hydraulic gradient increases, the flow velocity increases, the fluid flow will transition to turbulent flow when 10<*Re*, and Darcy's law fails. Forchheimer law is introduced when *Re*>10:

$$-\frac{dP}{dX}=\frac{\mu}{K}v+\beta\rho_w v^2, \tag{S19}$$

where β is the Forchheimer law coefficient, and $\beta=\frac{1.59\times10^3}{\sqrt{K}\phi^{5.5}}$:

To compare the analysis with Darcy's law, non–Darcy permeability K_N is introduced:

$$K_N=\frac{K}{1+\frac{\beta\rho_w K v}{\mu}}, \tag{S20}$$

Then, Eq. (S19) is simpled as:

$$-\frac{dP}{dX}=\frac{\mu}{K_N}v, \tag{S21}$$

The effective stress is altered with fluid pressure to associate the stress with the fluid, which results in stress sensitivity in the permeability and porosity of reservoir. Previous research (Wu, et al., 2019) has shown that the permeability of rock reduces exponentially as effective stress increases:

$$K=K_0e^{-M\sigma'}=K_0e^{-M(\sigma-\alpha P)}, \tag{S22}$$

where K_0 is the initial permeability, M is stress sensitivity factor of permeability (Hu, et al., 2020), σ' is the effective stress; P is the fluid pressure; σ is average stress.

The higher the stress sensitivity of porosity, the greater the proportion of interconnected pores that may be compressed. This leads to a positive relationship between the porosity and permeability (Hu, et al., 2020):

$$\frac{K}{K_0}=\left(\frac{\phi}{\phi_0}\right)^{\gamma}, \tag{S23}$$

where γ is porosity sensitivity exponent. In this study, $\gamma=3$.

Therefore, the stress sensitivity of porosity is obtained:

$$\phi=\phi_0e^{-\frac{M(\sigma-\alpha P)}{3}}, \tag{S24}$$

Section S3 Figures and table

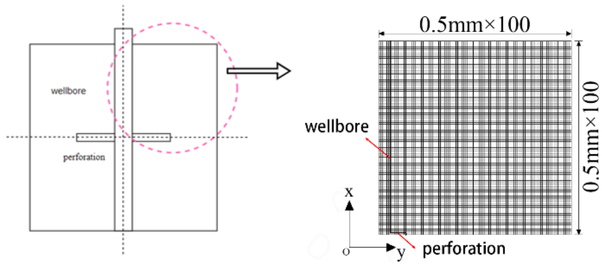

Fig. S3 The meshing of numerical model

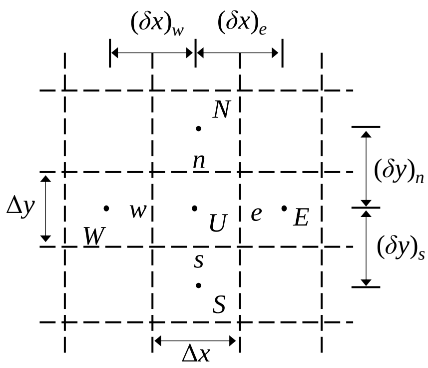

Fig. S4 Schematic diagram of grid system

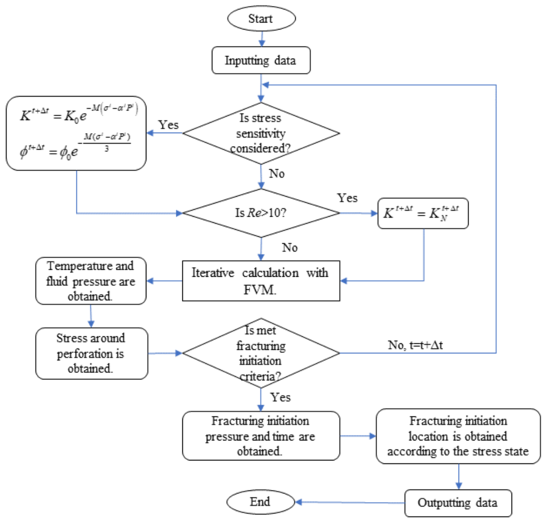

Fig. S5 Iterative calculation process of the numerical simulation method

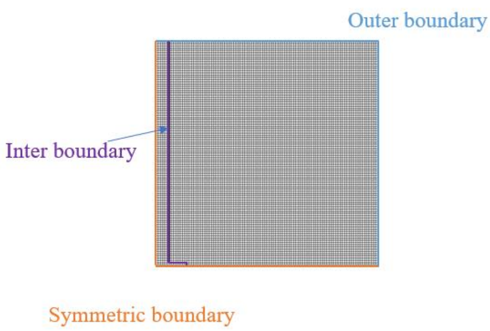

Fig. S6 Schematic diagram of boundary types

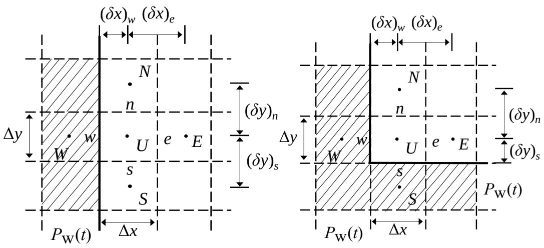

Fig. S7 Mesh system of inner boundary

Table S1 Simulation parameters

Parameter	Symbol	Value	From
Biot's coefficient	α	0.5428	–
Compressibility coefficient of reservoir (1/MPa)	α_0	0.45×10^{-9}	–
Thermal expansion coefficient (1/°C)	α_m	2.5×10^{-5}	–
Compressibility coefficient of fluid (1/MPa)	β_0	1×10^{-9}	–
Specific heat capacity of reservoir (Kj/(kg*°C))	C	0.84	–
Specific heat capacity of fluid (Kj/(kg*°C))	C_w	4.1868	–
Average thermal diffusivity (10^{-7}m^2/s)	D_T	7.15	(Chen and Ewy, 2005)
Elastic modulus (GPa)	E	$78.366e^{-0.0015T}$	(Xi and Zhao., 2010)
Initial porosity	ϕ_0	0.16	–
Initial permeability (m^2)	K_0	2.073×10^{-16}	–
Thermal conductivity (W/(m·K))	λ	5	(Chen and Ewy, 2005)
Modulus of Stress Sensitivity(1/MPa)	M	0.02	(Wu, et al., 2019)
Poisson's ratio of the reservoir	μ	$0.0699\ln T$ $+0.0028$	(Xi and Zhao., 2010)
Reservoir density (kg/m^3)	ρ	2650	–
Maximum in–situ horizontal stress (MPa)	σ_H	48	–
Minimum in–situ horizontal stress (MPa)	σ_h	40	–
Tensile strength (MPa)	σ_t	3.67	(Eshiet et al., 2012)
Vertical in–situ stress (MPa)	σ_v	50	–
Injection temperature (°C)	T_0	14	–
Initial flow rate (10^{-16}m^2)	v_0	2.7	–

Reference

Chen G, Ewy RT, 2005. Thermoporoelastic Effect on Wellbore Stability. *SPE J.* 10, 121–129. https://doi.org/10.2118/89039-PA

Eshiet KI, Sheng Y, Ye J, 2012. Microscopic modelling of the hydraulic fracturing process. *Environmental Earth Sciences*, 68(4):1169-1186.
https://doi.org/10.1007/s12665-012-1818-5

Farahani H, M Yu, S Miska, and N Takach. 2006. Modeling Transient Thermo-Poroelastic Effects on 3D Wellbore Stability. SPE Annual Technical Conference and Exhibition.
https://doi.org/10.2118/103159-MS

Hu Z, Klaver J, Schmatz J, et al., 2020. Stress sensitivity of porosity and permeability of cobourg limestone. *Engineering Geology*, 273
https://doi.org/10.1016/j.enggeo.2020.105632

Wu Z, Cui C, Trivedi J, et al. 2019. Pressure analysis for volume fracturing vertical well considering low-velocity non-darcy flow and stress sensitivity. *Geofluids*, 2019:1-10.
https://doi.org/10.1155/2019/2046061

Xi B, Zhao Y., 2010. Experimental study of thermophysico-mechanical property of drilling surrounding rock in granite under high temperature and high pressure. *Chinese Journal of Rock Mechanics and Engineering*, 29(6):1245-1252